Citation: CPT Pharmacometrics Syst. Pharmacol. (2016) 5, 173–181; doi:10.1002/psp4.12057

ORIGINAL ARTICLE

PK-PD Modeling of Individual Lesion FDG-PET Response to Predict Overall Survival in Patients With Sunitinib-treated Gastrointestinal Stromal Tumor

E Schindler[1]*, MA Amantea[2], MO Karlsson[1] and LE Friberg[1]

Pharmacometric models were developed to characterize the relationships between lesion-level tumor metabolic activity, as assessed by the maximum standardized uptake value (SUV_{max}) obtained on [^{18}F]-fluorodeoxyglucose (FDG) positron emission tomography (PET), tumor size, and overall survival (OS) in 66 patients with gastrointestinal stromal tumor (GIST) treated with intermittent sunitinib. An indirect response model in which sunitinib stimulates tumor loss best described the typically rapid decrease in SUV_{max} during on-treatment periods and the recovery during off-treatment periods. Substantial interindividual and interlesion variability were identified in SUV_{max} baseline and drug sensitivity. A parametric time-to-event model identified the relative change in SUV_{max} at one week for the lesion with the most pronounced response as a better predictor of OS than tumor size. Based on the proposed modeling framework, early changes in FDG-PET response may serve as predictor for long-term outcome in sunitinib-treated GIST.
CPT Pharmacometrics Syst. Pharmacol. (2016) **5**, 173–181; doi:10.1002/psp4.12057; published online 16 March 2016.

Study Highlights

WHAT IS THE CURRENT KNOWLEDGE ON THE TOPIC? ☑ Previously developed PK-PD models identified sunitinib-induced changes in the soluble VEGFR 3, neutrophil counts, and blood pressure as predictors of OS in patients with GIST. Changes in tumor metabolic activity, occurring several weeks before changes in tumor size, may also correlate to clinical outcome in GIST treated with anti-angiogenic drugs. • WHAT QUESTION DID THIS STUDY ADDRESS? ☑ A pharmacometric modeling framework linking sunitinib exposure, longitudinal lesion-level tumor metabolic activity, tumor size, and OS was developed. The predictive ability of tumor metabolic activity and tumor size on OS was investigated. • WHAT THIS STUDY ADDS TO OUR CURRENT KNOWLEDGE ☑ The developed model described the schedule-dependent tumor metabolic response and quantified substantial interlesion variability. Larger changes in metabolic activity in the lesion that best responds after one week predicted longer OS. • HOW THIS MIGHT CHANGE CLINICAL PHARMACOLOGY AND THERAPEUTICS ☑ Tumor metabolic activity is a promising marker for early assessing response to sunitinib. The developed modeling framework may be used to support dose and schedule selection for anti-angiogenic compounds.

Gastrointestinal stromal tumors (GISTs) are soft tissue sarcomas that respond poorly to conventional cytotoxic chemotherapies and palliative radiotherapy. The treatment of unresectable and metastatic GIST has substantially improved with the introduction of targeted agents, such as imatinib mesylate and sunitinib malate. Sunitinib is an oral, multitargeted tyrosine-kinase inhibitor approved multinationally for the treatment of imatinib-resistant or imatinib-intolerant GIST, advanced renal cell carcinomas and pancreatic neuroendocrine tumors.[1] Sunitinib inhibits platelet-derived growth factor receptors α and β, the stem cell factor receptor (KIT), the vascular endothelial growth factor receptors (VEGFRs; VEGFR-1, VEGFR-2, and VEGFR-3), and several other tyrosine kinase receptors. Sunitinib predominantly exhibits cytostatic and antiangiogenic effects, explaining that pronounced tumor shrinkage is rare when assessed by the Response Evaluation Criteria in Solid Tumors based on the sum of longest diameters (SLD) of target lesions.[2] Sunitinib provides, however, significant clinical benefit and prolongs survival.[3,4] Therefore, anatomic size changes may be insufficient to assess biological activity of cytostatic drugs[5] and pharmacodynamic (PD) circulating and imaging biomarkers are considered valuable adjuncts to tumor size to monitor therapeutic response.

By elucidating the relations between drug exposure, PD responses, and clinical outcomes, pharmacometric modeling helps in identifying new biomarkers of response and guiding oncology clinical trial design and therapeutic decisions.[6–8] Hansson *et al.*[9,10] developed a population pharmacokinetic (PK)-PD modeling framework for sunitinib treated patients with GIST linking drug exposure to the time-course of circulating biomarkers (vascular endothelial growth factor [VEGF], the soluble VEGF receptors sVEGFR-2 and sVEGFR-3, and soluble KIT [sKIT]), SLD, adverse effects (fatigue, hand-foot syndrome, neutropenia, and hypertension) and overall survival (OS). Sunitinib induced a schedule-dependent increase in VEGF and decrease in sVEGFR-2, sVEGFR-3, and sKIT. The

[1]Department of Pharmaceutical Biosciences, Uppsala University, Uppsala, Sweden; [2]Pfizer Inc., La Jolla, California, USA. *Correspondence: Emilie Schindler (emilie.schindler@farmbio.uu.se)
Received 27 August 2015; accepted 17 December 2015; published online on 16 March 2016. doi:10.1002/psp4.12057

Table 1 Summary of study design and study assessments

Characteristics	Description
Study design	Open-label, multicenter, dose escalation, phase I/II study
Total no. of patients	66
Dosing schedule, wk on/off: starting daily dose, mg q.d. [*N*]	2/1: 50 [$N=6$]
	2/2[a]: 25 [$N=6$][b], 50 [$N=24$], 75 [$N=3$][c]
	4/2: 50 [$N=27$]
FDG-PET assessment time, study day	2/1: cycle 1: 0, 7, 21; cycle 8: 14
	2/2: cycle 1: 0, 7, 28; cycle 4: 28
	4/2: cycle 1: 0, 7, 42; cycle 4: 28
SLD assessment time, study day	2/1: cycle 1: 0; cycle 4, 8, 12: 14
	2/2: cycle 1: 0; cycle 2 and every other cycle: 28
	4/2: cycle 1: 0; cycle 2 and every other cycle: 28

FDG, fluorodeoxyglucose; PET, positron emission tomography; SLD, sum of longest diameters.
[a]Ten patients who began treatment on schedule 2/2 switched to schedule 4/2 after completing 8 to 21 cycles.
[b]All patients who began treatment at 25 mg daily were switched to 50 mg daily at cycle 2 or 3.
[c]All patients who began treatment at 75 mg daily were switched to 50 mg daily during or at the end of cycle 1.

sVEGFR-2 and sVEGFR-3 turnover times were highly correlated as well as their drug sensitivities. The sVEGFR-3 and sKIT relative change from baseline, in addition to sunitinib exposure, successfully described SLD time-course. A smaller baseline SLD and larger sVEGFR-3 change from baseline were associated with longer OS.

Functional imaging by [^{18}F]-fluorodeoxyglucose (FDG) positron emission tomography (PET) has been proposed to complement tumor size to assess early response to therapy in GIST[11–13] and for cytostatic drugs.[5] Most GISTs exhibit a high glycolytic activity and therefore a marked FDG uptake, as assessed by the maximum standardized uptake value (SUV_{max}) of a region of interest (ROI).[14] A decrease in SUV_{max} shortly after sunitinib treatment initiation (1–4 weeks) has been suggested to correlate with clinical outcome.[3,15] Other FDG-PET metrics, such as mean standardized uptake value (SUV_{mean}), reflecting the overall tumor proliferation, have also been proposed but may be associated with more variability because of manual ROI selection.[14] Moreover, owing to tumor heterogeneity, SUV_{mean} do not always correlate with SUV_{max}; hence, further studies are warranted to identify the most predictive measure. In the present work, relationships between sunitinib exposure and the time-course of individual lesion SUV_{max} and SUV_{mean} in GIST were assessed using pharmacometric models, in which both interindividual and interlesion variability were characterized. Relationships between SUV, biomarkers, SLD, and OS were explored.

METHODS

Patients and data

Data from 66 adult patients with imatinib-resistant or imatinib-intolerant GIST treated with sunitinib in a phase I/II study were analyzed.[3] Sunitinib was administered orally once daily according to dosing schedules described in **Table 1**. FDG-PET data were available from baseline and at least one postbaseline scan (**Table 1**). Whole-body PET-scanning had been performed in a fasting-state 60 minutes after FDG administration. SUV corrected for lean body mass was calculated for a maximum of six reference lesions evaluable at baseline by computed tomography or magnetic resonance imaging (MRI). SUV_{max} (SUV of the most active voxel in an ROI) and SUV_{mean} (mean SUV for all voxels in an ROI) were recorded for each lesion.[14] SLD and biomarkers data (VEGF, sVEGFR-2, and sKIT) were also collected. Lesions included in SUV and SLD calculations could differ. Written informed consent was obtained from all patients. The study was approved by the institutional review boards of the participating institutions.

Model development

Pharmacometric models were developed using the nonlinear mixed-effect modeling software NONMEM version 7.3.[16] The first-order conditional estimation method with interaction and, for dropout and OS analyses, the Laplacian estimation method was used for parameter estimation. Data preprocessing and postprocessing, model diagnostics, and graphical visualization were performed using R software version 2.15.3, the R-based module Xpose version 4, the PsN toolkit version 4, and Piraña version 2.9.0.[17]

Model discrimination was based on graphical diagnostics and comparison of the objective function value (OFV, −2*log-likelihood). The OFV difference (dOFV) between nested models is approximately χ^2 distributed with degrees of freedom being the difference in number of parameters. A significance level of $P<0.05$ was used to discriminate between nested models. Relative standard errors (RSEs) of parameter estimates were obtained from the NONMEM Sandwich matrix for continuous data, and from the R matrix for dropout and OS models. The predictive performance of the individual lesion SUV and SLD models was assessed using visual predictive checks (VPCs), in which 95% confidence intervals derived from 500 simulated datasets were compared to the observed data. Kaplan–Meier VPCs, comparing the 95% confidence interval derived from 200 simulations to the observed OS data, were used to evaluate the performance of the OS model.

Pharmacokinetics

Sunitinib daily dose and daily area under the concentration-time curve (AUC_{daily}), calculated as daily dose/(CL/F), were investigated as drivers in the PD models. Individual empirical Bayes estimates for the apparent oral clearance (CL/F) were obtained from a published PK model.[18] When no PK data were available ($N=22$), CL/F typical population value corrected for gender, race, and tumor type (GIST) was used. During off-treatment periods, AUC_{daily} was assumed to be zero. PK data for the equipotent metabolite SU12662 were not available.

Individual lesion SUV_{max} model

SUV_{max} time-course was initially explored for an exponential increase in absence of drug, as described in the growth models proposed by Claret *et al*.[19] Alternatively, indirect response (IDR) models were investigated,[20] in which the

response is assumed to be at steady state (baseline) in the absence of drug and returns to baseline when the drug washes out. The IDR model best characterized the data (lower OFV) and was therefore selected for further assessment. IDR models with inhibition of the zero-order production (R_{in}) or stimulation of the first-order loss of response (k_{out}) were evaluated to characterize the time-course of individual lesions SUV_{max}, which typically decrease during sunitinib treatment. Linear, power, and E_{max} drug-effect relationships were considered. An effect compartment accounted for sunitinib accumulation and long elimination half-life ($T_{1/2,el}$~50 hours).[21] Because of the study design, the equilibration half-life ($T_{1/2,ke0}$) could not be estimated and was fixed to 50 hours. Linear and nonlinear disease progression models allowing for an underlying increase in SUV_{max} during the study were tested. Additionally, a mono-exponential time-dependent decay in drug effect was tested. Interindividual and interlesion variability were evaluated for all model parameters.

Assuming that data were collected for L lesions, j = 1, 2... L, the model parameter for the i^{th} subject (θ_i) can be written as:

$$\theta_i = \begin{cases} \theta \cdot \exp(\eta_i + \kappa_1) & \text{if lesion 1} \\ \theta \cdot \exp(\eta_i + \kappa_2) & \text{if lesion 2} \\ \vdots & \\ \theta \cdot \exp(\eta_i + \kappa_L) & \text{if lesion L} \end{cases} \quad (1)$$

where θ is the typical parameter value in the population. η_i, the random effect common to all lesions for the ith subject, is assumed to be normally distributed with mean 0 and variance ω^2. κ_j, the random effect specific to the jth lesion, is assumed to be normally distributed with mean 0 and variance π_j^2. A common variance was assumed for all lesions ($\pi_1^2 = \pi_2^2 = \cdots = \pi_j^2$).

Sources of residual variability on SUV_{max} may affect all lesions assessed on the same FDG-PET scan (e.g., injected radioactivity concentration, scanner resolution) or a single lesion (e.g., ROI determination). NONMEM level-2 item was used to group together observations from lesions assessed on the same scan. These observations were allowed to have different residual error values (ε), arising from a multivariate normal distribution parameterized with a zero mean vector and a covariance matrix Σ. The diagonal elements of Σ corresponding to the variances for each ε were assumed to be the same. The off-diagonal elements of Σ displaying the covariances between ε were assumed to be the same, denoting the same correlation between the residual errors for all lesions assessed simultaneously. This was implemented in NONMEM through a Cholesky decomposition of the sigma matrix (see **Supplementary Material**).

As SUV_{mean} and SUV_{max} data were highly correlated ($r^2 = 0.96$), the SUV model was built using SUV_{max} data, the most commonly reported SUV metrics.[22] The best model structure was then applied to SUV_{mean} data and parameters were re-estimated.

Correlations between SUV_{max} and SLD

Individual lesion SUV_{max} and SLD data were modeled jointly using the best structural model for individual lesion SUV_{max} combined with a tumor growth inhibition model describing SLD.[19] The tumor growth inhibition model included an exponential growth, a linear drug effect driven by AUC_{daily} (through the effect compartment) that increases tumor death rate, and a mono-exponential function accounting for drug effect diminution over time to explain tumor progression or resistance appearance. Exponential interindividual variability terms were included in SLD baseline, the growth rate constant, and the drug effect. All fixed and random effects parameters in the SUV_{max}-SLD model were estimated simultaneously. Correlations at the individual level between model parameters were investigated.

Correlations between SUV_{max} and biomarkers

The best structural model for individual lesion SUV_{max} was combined with a previously developed joint model for biomarkers.[9] The biomarkers' time-courses were described by IDR models in which sunitinib inhibited VEGF degradation and sVEGFR-2 and sKIT production. Sigmoidal I_{max} (VEGF, sVEGFR-2) and I_{max} (sKIT) models described the drug-effect relationships. A time-dependent linear disease progression model accounted for the observed VEGF increase and sKIT decrease from baseline over time. All fixed and random effects parameters in the SUV_{max}-biomarker model were estimated simultaneously. Correlations at the individual level between model parameters were investigated.

Overall survival model

OS data were analyzed using parametric time-to-event models.[23] Exponential and Weibull distributions were evaluated to describe the baseline hazard ($h_0(t)$). Predictors were tested one by one and in combination on the hazard h(t) (Eq. 2).

$$h(t) = h_0(t) \cdot e^{\beta_1 \cdot x_1 + \cdots + \beta_n \cdot x_n} \quad (2)$$

where β_i (i = 1,...,n) are coefficients representing the size of the effect of a set of predictors (x_1, ..., x_n).

Baseline predictors included the number of FDG-PET positive lesions, Eastern Cooperative Oncology Group functional status, baseline SLD, and the summed SUV_{max} across lesions (ΣSUV_{max}). The predictive ability of time-varying predictors including AUC_{daily}, the model-predicted time-courses of ΣSUV_{max}, of SUV_{max} of the most active (hottest) lesion, and of SLD were investigated. The product of SLD and ΣSUV_{max} and the product of SLD and ΣSUV_{mean} were also tested. Moreover, the model-predicted relative changes in ΣSUV_{max} and SLD from baseline over time were evaluated. Dose and time-varying predictors were extrapolated assuming that patients were treated with sunitinib until the time of death or censoring according to their last dose and dosing schedule even after tumor progression, as no other treatment option was available at the time of the study and the protocol supported continuation of treatment. Additionally, the relative change in ΣSUV_{max} at week one or two and the relative change in SUV_{max} for the lesion that responded the best ($RCFB_{max}$) at week one or two were tested.

Table 2 Final individual lesion SUV_{max}, SLD, dropout, and overall survival model parameter estimates

Parameter	Typical value (RSE %)	Interindividual variability CV % (RSE %)	Interlesion variability CV % (RSE %)
Individual lesion SUV_{max} model			
SUV_0	7.59 (5.9)	32 (16)	23 (16)
k_{out} (wk^{-1})	0.556 (29)	–	–
$DRUG_{SUV}$ ($mg^{-1}.L.h^{-1}$)	0.946 (15)	74 (26)	57 (20)
Residual error (%)	41.7 (20)	–	–
SLD model			
SLD_0 (mm)	263 (6.8)	54 (9.6)	–
K_{GROW} (wk^{-1})	0.0105 (24)	60 (38)	
$DRUG_{SLD}$ ($mg^{-1}.L.h^{-2}$)	0.0166 (21)	63 (37)	–
λ (wk^{-1})	0.0201 (45)	–	–
Residual error (%)	6.68 (12)	–	–
Correlation $DRUG_{SUV}/DRUG_{SLD}$ (%)	85.1 (22)	–	–
OS model			
h_0 (wk^{-1})	0.0191 (3.1)		
β	5.36 (8.5)	–	–

β, parameter relating the maximum relative change from baseline in individual lesion SUV_{max} at week one to the hazard; CV, coefficient of variation; $DRUG_{SLD}$, tumor size reduction rate constant; $DRUG_{SUV}$, slope of the linear drug effect on SUV_{max}; h_0, constant baseline hazard for the overall survival model; K_{GROW}, tumor growth rate constant; k_{out}, SUV_{max} turnover rate constant; OS, overall survival; λ, rate constant for drug effect washout; RSE, relative standard error; SLD, sum of longest diameters; SLD_0, baseline sum of longest diameters; SUV_{max}, maximal standardized uptake value; SUV_0, estimated individual lesion SUV_{max} at baseline.

A time-to-event model described censoring, defined as loss to follow-up or nonoccurrence of death at the end of the study, to account for varying follow-up durations.

$$\frac{dC_e}{dt} = k_{e0} \cdot \left(AUC_{daily} - C_e\right) \quad (3)$$

$$\frac{dSUV_{max}}{dt} = R_{in} - k_{out} \cdot (1 - DRUG_{SUV} \cdot C_e) \cdot SUV_{max}(t) \quad (4)$$

$$R_{in} = SUV_{max,0} \cdot k_{out} \quad (5)$$

RESULTS

Patients and data

Baseline and postbaseline SUV_{max} and SUV_{mean} data ($n = 620$) were available in 66 patients for up to 102 weeks of treatment (median follow-up time of 10 weeks). One to five target lesions were followed for each patient, resulting in a total of 176 lesions. Three lesions from two different patients could not be imaged after the third visit and were handled as below the quantification limit, setting the first missing SUV to half of the lowest value in the dataset, and ignoring the following missing data.[24] Dosing history, SLD, and OS data were available for all patients and 36 patients (55%) had biomarker data.

Joint model for individual lesion SUV_{max} and SLD

Data exploratory analysis showed schedule-dependent changes in individual lesion SUV_{max} and SUV_{mean}, with a decrease during on-treatment periods and a recovery during off-treatment periods. Log-transformed individual lesion SUV_{max} data were best described by an IDR model with stimulation of k_{out}. An IDR model with inhibition of R_{in}, with E_{max} drug-effect assuming a maximum inhibition had similar OFV (dOFV = −4.0 for the same number of parameters) but demonstrated poorer simulation properties and was therefore not selected. The linear drug-effect was driven by AUC_{daily} through an effect compartment (Eqs. 3–5). A disease progression component or a time-dependent decay in drug effect was not significant.

Interindividual and interlesion variability were significant to include in the baseline ($SUV_{max,0}$) and the drug effect parameter ($DRUG_{SUV}$). For both parameters, interindividual variability was estimated to be larger than interlesion variability, although interlesion variability was of significance (32% interindividual and 23% interlesion variability for $SUV_{max,0}$, and 74% interindividual and 57% interlesion variability for $DRUG_{SUV}$).

In the individual lesion SUV_{max}-SLD joint model, parameters were estimated with acceptable precision (RSE ≤29% for fixed effects, ≤38% for random effects) except for the rate constant for vanishing drug effect on SLD, λ (45%). Removal of λ increased the OFV by 60 points and the function was therefore kept in the model. Parameter estimates and their uncertainty are summarized in **Table 2**. The drug effects on individual lesion SUV_{max} and SLD were 85% correlated at the individual level. The model predicts a typical turnover time ($1/k_{out}$) of SUV_{max} of 1.8 weeks, and typical decreases in SUV_{max} of 26% and 47% after one and two weeks of sunitinib treatment (50 mg q.d.), respectively.

Graphical exploration of dropout patterns showed no evidence that dropout from FDG-PET measurements was related to the magnitude of SUV_{max}. Therefore, the realized study design was used for simulations to generate VPCs of individual lesion SUV_{max}. For SLD simulations a previously published dropout model[9] accounted for the probability of dropping out from SLD assessments. The logistic regression dropout model included as predictors the observed SLD at dropout and a >20% increase in SLD from nadir

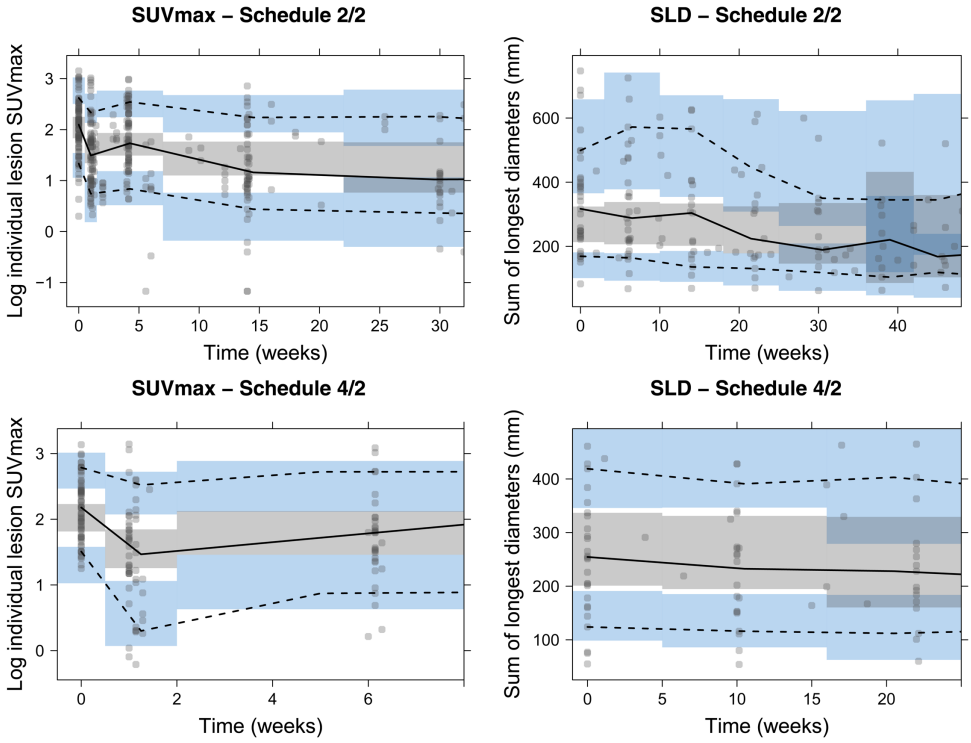

Figure 1 Visual predictive checks of the joint model for individual lesion maximum standardized uptake value (SUV_{max}, left panels) and the sum of longest diameters (SLD; right panels) for dosing schedules 2/2 (top) and 4/2 (bottom). Median (solid line), 10th and 90th percentiles (dashed lines) of the observed data are compared to the 95% confidence intervals (shaded areas) for the median (gray), 10th and 90th percentiles (blue) of the simulated data (based on 500 simulations). The dots represent the observed data.

(yes/no). Time since first dose was not significant in the present study. VPCs for the best individual lesion SUV_{max}-SLD model showed a good predictive performance of the joint model (**Figure 1**, **Supplementary Figure**).

The individual lesion SUV_{max} model structure was successfully applied to individual lesion SUV_{mean} data. The typical value of the drug effect parameter in SUV_{mean} model and its interindividual and interlesion variability ($0.920\ mg^{-1} \cdot L.h^{-1}$, 77% coefficient of variation, and 57% coefficient of variation, respectively) were of similar magnitude as for SUV_{max}.

Joint model for individual lesion SUV_{max} and biomarkers

A joint model for individual lesion SUV_{max}, VEGF, sVEGFR-2, and sKIT was developed using data from 36 patients with available biomarkers data. As there was limited information on disease progression in the data, the typical value of the slope in the linear disease progression for VEGF and sKIT was fixed to the published value ($0.0261\ month^{-1}$). No statistically significant correlations between parameters in the SUV_{max} and biomarker models were identified.

Overall survival model

OS data were collected up to 102 weeks. Eleven patients (17%) had an event. Individual lesion SUV_{max}, SLD, and OS data were fitted simultaneously.[25,26] The population SUV_{max} and SLD parameters were fixed to the values from the best SUV_{max}-SLD model, but individual SUV_{max} and SLD parameters were estimated simultaneously with OS parameters based on all data, similar to the PPP&D approach described by Zhang *et al*.[27] The probability of OS was best described by an exponential distribution (constant hazard). The probability of being censored was described by a time-to-event model with constant hazard. In the univariate analysis, $RCFB_{max}$ at one week (dOFV = −8.8) and two weeks (dOFV = −4.5) were identified as significant predictors of OS. AUC_{daily} achieved statistical significance but resulted in model instability and the 95% confidence interval around the estimate of the size of AUC_{daily} effect on the hazard included zero. The model-predicted SLD time-course (dOFV = −7.8) and relative change in SLD from baseline over time (dOFV = −6.6) also resulted in a significant OFV drop; however, these drops were driven by a single individual. When $RCFB_{max,wk1}$ was included in the model, none of the other predictors further improved model fit. Eq. 6 describes the hazard function for the best OS model:

$$h(t) = h_0 \cdot e^{\beta \cdot RCFB_{max,wk1}} \quad (6)$$

where h_0 represents the constant baseline hazard and β the size of the effect of $RCFB_{max,wk1}$ on the hazard. β was estimated to 5.36, corresponding to a hazard ratio (HR) of 0.16, 0.02, and 0.50 for the median (−0.34), 5th (−0.76), and 95th (−0.13) percentiles of $RCFB_{max,wk1}$, respectively. Uncertainty around the HR was reasonable (95% confidence interval = 0.12–0.22 for the median $RCFB_{max,1wk}$).

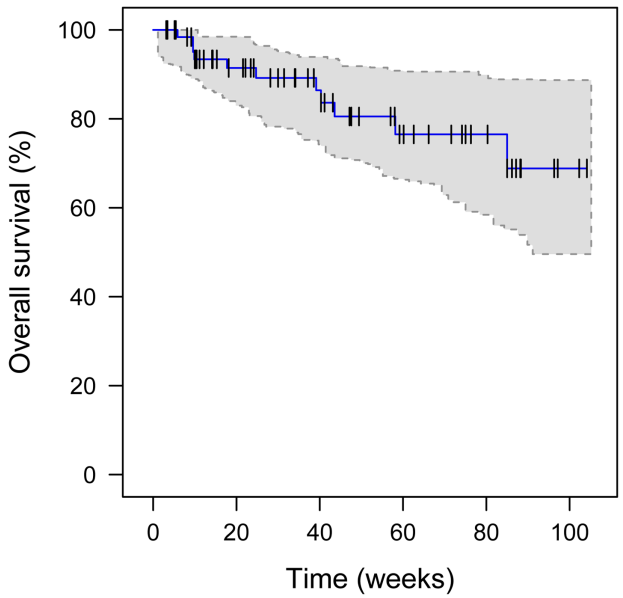

Figure 2 Kaplan–Meier visual predictive checks of the overall survival model. The blue line represents the observed Kaplan–Meier curve and the black ticks represent censored events. The gray shaded area is the 95% confidence interval of the simulated data (200 simulations).

Similar results were obtained when assessing the predictive ability of SUV_{mean}. Kaplan–Meier VPCs showed a good performance of the model (**Figure 2**).

DISCUSSION

In this pharmacometric analysis, the time-course of tumor metabolic activity assessed by FDG-PET after sunitinib treatment in patients with GIST was described and substantial interindividual and interlesion variability in FDG-PET response were estimated. Correlations between sunitinib effects on tumor metabolic activity and tumor size, but not circulating biomarkers, were identified. An early FDG-PET response was predictive of OS with an HR of 0.16 for a median relative decrease in SUV_{max} from baseline at week one of 34%. Even though the individual drug effect parameters on SUV_{max} and SLD were highly correlated, the magnitude of change and the onset time are different, explaining why FDG-PET was better than SLD at predicting OS. **Figure 3** illustrates the developed modeling framework.

Lesion-level SUV_{max} data were best characterized by an IDR model in which sunitinib stimulated the loss of SUV_{max} response. Little is known about the mechanistic rationale behind the sunitinib-induced decrease in tumor FDG uptake. Possible mechanisms include a deprivation of tumor accessibility to glucose due to the anti-angiogenic effect[28] and a reduced expression of glucose transporters 1. As sunitinib inhibits multiple tyrosine kinases, other pathways may be involved in its metabolic effects on tumors. As new data become available, an IDR model with inhibition of response production may be reevaluated.

In our analysis, an IDR model could characterize SUV_{max} time-course significantly better than an exponential growth model. The latter could capture the initial decrease in SUV_{max} but not the rapid recovery during off-treatment periods. These results contrast with findings in erlotinib-treated patients with nonsmall cell lung cancer,[29] in which the peak SUV (SUV_{peak}, SUV within a 1 cm^3-sphere centered in the highest-uptake region) time-course assessed by FDG-PET and 3′-[18F]fluoro-3′-deoxy-L-thymidine (FLT)-PET was modeled. The authors used a tumor progression inhibition model to characterize the changes among baseline, week one, and week six in SUV_{peak} for the hottest lesion up to five lesions (not necessarily the same lesion at each timepoint). Erlotinib continuous daily dosing and the short study duration may explain why a tumor progression inhibition model described their data but could not appropriately characterize the SUV data in the current study. Additionally, a waning of the drug effect accounting for disease progression or resistance appearance was identified for SUV_{peak} in nonsmall cell lung cancer, whereas it was not significant in the present analysis.

To the best of our knowledge, this is the first analysis in which the interindividual variability has been separated from the interlesion variability and from residual variability in a single estimation process. The methodology presented herein could be applied to other lesion-level tumor data, for example, individual lesion tumor diameters or volumes. Ferl *et al*.[30] proposed a model for dynamic contrast-enhanced magnetic resonance imaging (DCE-MRI) biomarkers lesion-level data in patients with liver metastases from primary epithelial colorectal cancer after a single administration of bevacizumab, an anti-VEGF monoclonal antibody. The individual lesion baseline biomarker values were estimated as a function of the observed baseline and a lesion-specific residual variability magnitude.[31] However, the interlesion variability could not be separated from the residual unexplained variability. With our approach, the effect of potentially available covariates (e.g., lesion localization, mutation status) could be explored to explain part of the variability in response between lesions. Unfortunately, such data were not available in the present study.

When the individual lesion SUV_{max} was modeled jointly with VEGF, sVEGFR-2, and sKIT, no significant correlations were identified between the baseline levels or the sensitivity to sunitinib for the different variables. Sunitinib inhibits several tyrosine kinase receptors involved in various molecular pathways and results in both anti-angiogenic and antitumor effects.[1] The absence of correlations may be due to heterogeneous levels of inhibition of these pathways within a patient. However, as circulating biomarker data were only collected in 36 patients, these results should be treated with caution.

The typical predictions (relative to baseline) derived from the individual lesion SUV_{max}-SLD model, after treatment with 50 mg of sunitinib on 4/2 and 2/2 schedules, are depicted in **Figure 4**. The model predicts a rapid and pronounced decrease in SUV_{max} after sunitinib administration, whereas the change in SLD is predicted to be slower and of a smaller magnitude during the observation period.

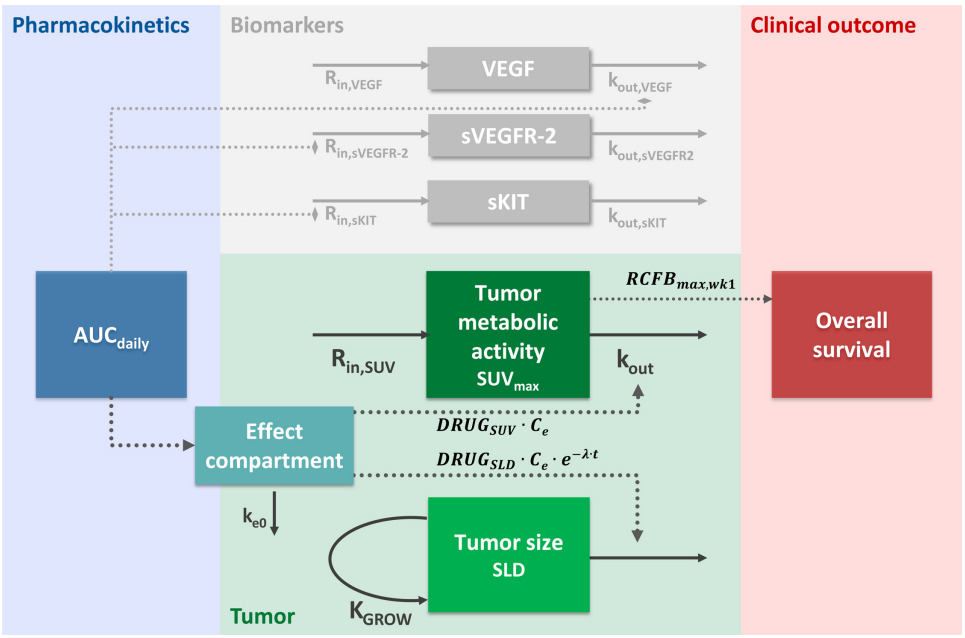

Figure 3 Schematic representation of the modeling framework for sunitinib in gastrointestinal stromal tumor patients. Dashed arrows represent effects identified as statistically significant. Sunitinib daily area under the curve (AUC_{daily}) was used as a driver of the drug effect on tumor metabolic activity, assessed by [^{18}F]-fluorodeoxyglucose positron emission tomography (FDG-PET) as the maximal standardized uptake value (SUV_{max}), tumor size (sum of longest diameters [SLD]) and biomarkers (the soluble stem cell factor receptor [sKIT], the soluble vascular endothelial growth factor receptor [sVEGFR-2], and the vascular endothelial growth factor [VEGF]). An effect compartment accounted for sunitinib long half-life. SUV_{max} was described by a turnover model where sunitinib stimulates the loss of SUV_{max} response. SLD model included an exponential growth and a washout of the drug effect over time. Biomarkers time-courses were described by published turnover models [Hansson *et al*.[9,10]]. The drug effect on SUV_{max} ($DRUG_{SUV}$) and SLD ($DRUG_{SLD}$) were positively correlated, whereas no correlations were found between SUV_{max} and biomarkers responses. The relative change in SUV_{max} from baseline after one week of treatment for the lesion that best responds to sunitinib was a significant predictor of overall survival. k_{e0}, equilibration constant for the effect compartment; K_{GROW}, first-order growth rate constant; k_{out}, first-order rate constant for the loss of response; λ, rate constant for the disappearance of drug effect on SLD; R_{in}, zero-order rate constant for the production of response.

Despite the sparse data and rather small population, the parametric time-to-event model reported here successfully identified predictors for OS (i.e., a more pronounced change in SUV_{max} for the lesion that responds the best within a patient, as predicted by our model, was associated with longer OS). An HR of 0.59 is predicted for every 10% drop in SUV_{max} after one week of treatment. These results are comparable to the findings in erlotinib-treated nonsmall cell lung cancer, in which the relative change from baseline in SUV_{peak} after one week was associated with an improved OS, with an HR of 0.84 for every 10% drop in SUV_{peak}.[29] Altogether, these results indicate that FDG-PET can potentially serve as an early biomarker of tumor response to targeted treatments, and that early changes in SUV_{max} may be used as a predictor for long-term outcome (OS).

The data, as described by our model, indicate that sunitinib typically causes a rapid initial decrease in SUV_{max} followed by a recovery toward baseline during off-treatment periods. These findings may explain why observed FDG-PET response at week four did not correlate with clinical outcome in a study of sunitinib-treated patients with metastatic clear-cell renal cancer.[32] In that study, FDG-PET scans were assessed two to five days after the last dose in cycle one (i.e., tumor metabolic activity may have already increased during the period off-treatment and variability in response may be due to different assessment time). For future studies assessing FDG-PET response to drugs with intermittent schedules, trial designs should acknowledge potential schedule dependence of tumor metabolic response.

Other treatment schedules than the approved 4/2 schedule have been investigated in GIST and other solid tumors. George *et al*.[33] reported the results of a phase II study in imatinib-resistant patients with GIST assessing the efficacy and safety of sunitinib continuous daily dosing at a dose of 37.5 mg/day, chosen to achieve the same dose intensity over a six-week period. The continuous daily dosing schedule was associated with sustained effective drug concentrations, acceptable safety, and persistent effects on VEGF, sVEGFR-2, sVEGFR-3, and sKIT, without concentration rebounds observed during off-treatment periods with discontinuous schedules. Additional treatment schedules have been proposed for metastatic renal cell carcinoma in which individualized increases in sunitinib dose or longer on-treatment periods with shorter off-treatment periods can be decided based on individual patient toxicity. However, it remains unclear

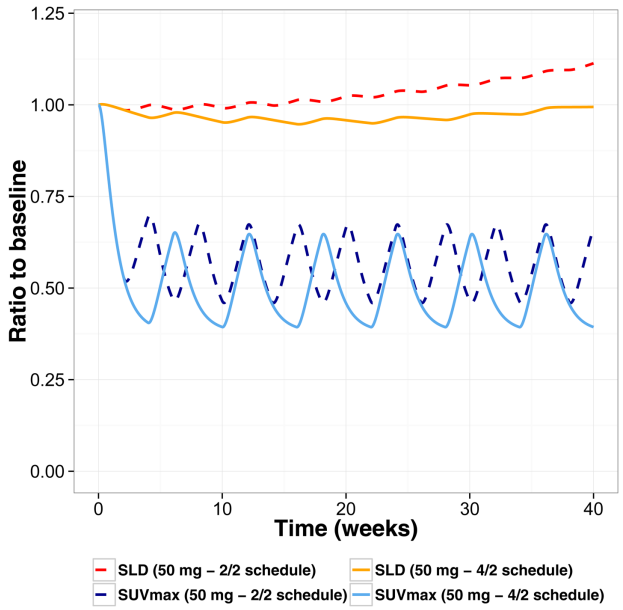

Figure 4 Typical predictions of the relative change from baseline in individual lesion maximum standardized uptake value (SUV_{max}) and the sum of longest diameters (SLD) during sunitinib treatment (50 mg q.d. on 2/2 and 4/2 weeks on/off schedule). The predictions were generated using the SUV_{max}-SLD joint model.

which dosing strategy is associated with the best clinical benefit.[34] Off-treatment periods are not only associated with tumor progression but also coincide with reemergence of tumor-related symptoms (e.g., coughing in patients with lung metastases).[35] Simulations using the developed modeling framework can help understand the tumor metabolic and anatomic response after different treatment schedules.

In summary, we have developed a model describing lesion-level FDG-PET data in sunitinib-treated patients with GIST followed up to 102 weeks. The SUV_{max}-SLD-OS joint model proposed here, together with the modeling framework proposed by Hansson *et al.*,[9,10] including biomarkers, SLD, adverse effects, and OS, offer a platform for performing simulations and investigating the effect of different treatment schedules and doses on clinical benefit and risk-benefit balance. This work may therefore support therapy individualization to improve the care of patients with cancer. Additionally, the developed framework can be used for leveraging the extensive clinical data collected throughout drug development, comparing the efficacy and safety profile of candidate drugs, and helping the selection of efficacious but safe doses.

Acknowledgments. The research leading to these results has received support from the Swedish Cancer Society, Sweden, and from the Innovative Medicines Initiative Joint Undertaking under grant agreement no. 115156, resources of which are composed of financial contribution from the European Union's Seventh Framework Programme (FP7/2007-2013), and EFPIA companies' in kind contribution. The DDMoRe project is also financially supported by contributions from Academic and SME partners.

Conflict of Interest. M.A.A. is an employee of Pfizer Ltd. M.O.K. and L.E.F. have acted as paid consultants to Pfizer Ltd. As Deputy Editor-in-Chief of *CPT: Pharmacometrics & Systems Pharmacology*, L.E.F. was not involved in the review or decision process for this article. E.S. declared no conflict of interest.

Author Contributions. E.S., M.A.A., M.O.K., and L.E.F. wrote the manuscript. E.S., M.A.A., M.O.K., and L.E.F. designed the research. E.S., M.A.A., M.O.K., and L.E.F. performed the research. E.S., M.A.A., M.O.K., and L.E.F. analyzed the data.

1. Rock, E.P. *et al.* Food and Drug Administration drug approval summary: sunitinib malate for the treatment of gastrointestinal stromal tumor and advanced renal cell carcinoma. *Oncologist* **12**, 107–113 (2007).
2. Eisenhauer, E.A. *et al.* New response evaluation criteria in solid tumours: revised RECIST guideline (version 1.1). *Eur. J. Cancer* **45**, 228–247 (2009).
3. Demetri, G.D. *et al.* Molecular target modulation, imaging, and clinical evaluation of gastrointestinal stromal tumor patients treated with sunitinib malate after imatinib failure. *Clin. Cancer Res.* **15**, 5902–5909 (2009).
4. Demetri, G.D. *et al.* Efficacy and safety of sunitinib in patients with advanced gastrointestinal stromal tumour after failure of imatinib: a randomised controlled trial. *Lancet* **368**, 1329–1338 (2006).
5. Contractor, K.B. & Aboagye, E.O. Monitoring predominantly cytostatic treatment response with 18F-FDG PET. *J. Nucl. Med.* **50** Suppl 1, 97S–105S (2009).
6. Bender, B.C., Schindler, E. & Friberg, L.E. Population pharmacokinetic-pharmacodynamic modelling in oncology: a tool for predicting clinical response. *Br. J. Clin. Pharmacol.* **79**, 56–71 (2015).
7. Mould, D.R., Walz, A.C., Lave, T., Gibbs, J.P. & Frame, B. Developing exposure/response models for anticancer drug treatment: special considerations. *CPT Pharmacometrics Syst. Pharmacol.* **4**, e00016 (2015).
8. Ribba, B. *et al.* A review of mixed-effects models of tumor growth and effects of anticancer drug treatment used in population analysis. *CPT Pharmacometrics Syst. Pharmacol.* **3**, e113 (2014).
9. Hansson, E.K. *et al.* PKPD modeling of VEGF, sVEGFR-2, sVEGFR-3, and sKIT as predictors of tumor dynamics and overall survival following sunitinib treatment in GIST. *CPT Pharmacometrics Syst. Pharmacol.* **2**, e84 (2013).
10. Hansson, E.K. *et al.* PKPD modeling of predictors for adverse effects and overall survival in sunitinib-treated patients with GIST. *CPT Pharmacometrics Syst. Pharmacol.* **2**, e85 (2013).
11. Van den Abbeele, A.D. The lessons of GIST–PET and PET/CT: a new paradigm for imaging. *Oncologist* **13** (suppl. 2), 8–13 (2008).
12. Treglia, G., Mirk, P., Stefanelli, A., Rufini, V., Giordano, A. & Bonomo, L. 18F-Fluorodeoxyglucose positron emission tomography in evaluating treatment response to imatinib or other drugs in gastrointestinal stromal tumors: a systematic review. *Clin. Imaging* **36**, 167–175 (2012).
13. Stefanelli, A., Treglia, G., Mirk, P., Muoio, B. & Giordano, A. F-FDG PET imaging in the evaluation of treatment response to new chemotherapies beyond imatinib for patients with gastrointestinal stromal tumors. *ISRN Gastroenterol.* **2011**, 824892 (2011).
14. Vanderhoek, M., Perlman, S.B. & Jeraj, R. Impact of different standardized uptake value measures on PET-based quantification of treatment response. *J. Nucl. Med.* **54**, 1188–1194 (2013).
15. Prior, J.O. *et al.* Early prediction of response to sunitinib after imatinib failure by 18F-fluorodeoxyglucose positron emission tomography in patients with gastrointestinal stromal tumor. *J. Clin. Oncol.* **27**, 439–445 (2009).
16. Beal, S., Sheiner, L.B., Boeckmann, A. & Bauer, R.J. NONMEM user's guides (1989–2009) (Icon Development Solutions, Ellicott City, MD, 2009).
17. Keizer, R.J., Karlsson, M.O. & Hooker, A. Modeling and simulation workbench for NONMEM: tutorial on Pirana, PsN, and Xpose. *CPT Pharmacometrics Syst. Pharmacol.* **2**, e50 (2013).
18. Houk, B.E., Bello, C.L., Kang, D. & Amantea, M. A population pharmacokinetic meta-analysis of sunitinib malate (SU11248) and its primary metabolite (SU12662) in healthy volunteers and oncology patients. *Clin. Cancer Res.* **15**, 2497–2506 (2009).
19. Claret, L. *et al.* Model-based prediction of phase III overall survival in colorectal cancer on the basis of phase II tumor dynamics. *J. Clin. Oncol.* **27**, 4103–4108 (2009).

20. Sharma, A. & Jusko, W.J. Characteristics of indirect pharmacodynamic models and applications to clinical drug responses. *Br. J. Clin. Pharmacol.* **45**, 229–239 (1998).
21. Papaetis, G.S. & Syrigos, K.N. Sunitinib: a multitargeted receptor tyrosine kinase inhibitor in the era of molecular cancer therapies. *BioDrugs* **23**, 377–389 (2009).
22. Wahl, R.L., Jacene, H., Kasamon, Y. & Lodge, M.A. From RECIST to PERCIST: evolving considerations for PET response criteria in solid tumors. *J. Nucl. Med.* **50** Suppl 1, 122S–150S (2009).
23. Holford, N. A time to event tutorial for pharmacometricians. *CPT Pharmacometrics Syst. Pharmacol.* **2**, e43 (2013).
24. Beal, S.L. Ways to fit a PK model with some data below the quantification limit. *J. Pharmacokinet. Pharmacodyn.* **28**, 481–504 (2001).
25. Ribba, B., Holford, N. & Mentré, F. The use of model-based tumor-size metrics to predict survival. *Clin. Pharmacol. Ther.* **96**, 133–135 (2014).
26. Desmée, S., Mentré, F., Veyrat-Follet, C. & Guedj, J. Nonlinear mixed-effect models for prostate-specific antigen kinetics and link with survival in the context of metastatic prostate cancer: a comparison by simulation of two-stage and joint approaches. *AAPS J.* **17**, 691–699 (2015).
27. Zhang, L., Beal, S.L. & Sheiner, L.B. Simultaneous vs. sequential analysis for population PK/PD data I: best-case performance. *J. Pharmacokinet. Pharmacodyn.* **30**, 387–404 (2003).
28. Calvo, M.B., Figueroa, A., Pulido, E.G., Campelo, R.G. & Aparicio, L.A. Potential role of sugar transporters in cancer and their relationship with anticancer therapy. *Int. J. Endocrinol.* **2010**, 205357 (2010).
29. Suleiman, A.A. *et al.* Modeling tumor dynamics and overall survival in advanced non-small-cell lung cancer treated with erlotinib. *J. Thorac. Oncol.* **10**, 84–92 (2015).
30. Ferl, G.Z. *et al.* Mixed-effects modeling of clinical DCE-MRI data: application to colorectal liver metastases treated with bevacizumab. *J. Magn. Reson. Imaging.* **41**, 132–141 (2015).
31. Dansirikul, C., Silber, H.E. & Karlsson, M.O. Approaches to handling pharmacodynamic baseline responses. *J. Pharmacokinet. Pharmacodyn.* **35**, 269–283 (2008).
32. Kayani, I. *et al.* Sequential FDG-PET/CT as a biomarker of response to sunitinib in metastatic clear cell renal cancer. *Clin. Cancer Res.* **17**, 6021–6028 (2011).
33. George, S. *et al.* Clinical evaluation of continuous daily dosing of sunitinib malate in patients with advanced gastrointestinal stromal tumour after imatinib failure. *Eur. J. Cancer* **45**, 1959–1968 (2009).
34. Bjarnason, G.A. *et al.* Outcomes in patients with metastatic renal cell cancer treated with individualized sunitinib therapy: correlation with dynamic microbubble ultrasound data and review of the literature. *Urol. Oncol.* **32**, 480–487 (2014).
35. Desar, I.M. *et al.* The reverse side of the victory: flare up of symptoms after discontinuation of sunitinib or sorafenib in renal cell cancer patients. A report of three cases. *Acta Oncol.* **48**, 927–931 (2009).

Supplementary information accompanies this paper on the *CPT: Pharmacometrics & Systems Pharmacology* website (http://www.wileyonlinelibrary.com/psp4)